

Near Field Scanning and Propagation of Correlated Low Frequency Radiated Emissions

Gabriele Gradoni, *Member, IEEE*, Deepthee Madenoor Ramapriya,
 Stephen C. Creagh, Gregor Tanner, Mohd Hafiz Baharuddin, Hayan Nasser, Christopher Smartt,
 and David W. P. Thomas, *Senior Member, IEEE*

Abstract—Electromagnetic radiation from complex printed circuit boards can occur over a broad frequency bandwidth, ranging from hundreds of MHz to tens of GHz. This is becoming a critical issue for assessment of EMC and interoperability as electronic components become more and more integrated. We use emissions from an enclosure with a single-slot aperture and equipped with operating electronics to exemplify and model such sources. Spatial correlation functions obtained from two-probe measurements are used both to characterise the source and to propagate the emissions. We examine emissions in the sub-microwave frequency range, where evanescent decay dominates the measured correlation function at the distances measured. We find that an approximate, diffusion-like propagator describes the measured emissions well. A phase-space approach based on Wigner functions is exploited to develop this approximation and to provide enhanced understanding of the emissions.

Index Terms—Statistical Electromagnetics, Near-field Scan, Wigner Function, Correlation, Radiated Emissions.

I. INTRODUCTION

Full characterisation of the field emissions of complex and highly integrated printed circuit boards (PCBs) requires measurements of space-time stochastic electromagnetic (EM) fields. Several methods have been proposed to characterise radiated emissions through near-field scanning (NFS) of deterministic fields [1], [2], [3], [4], [5]. Near-field measurements require less space, have better signal-to-noise ratios and are simpler than far-field measurements [5]. These methods have been inherited and adapted to predict the radiation of circuits and devices. More recently, statistical methods have been introduced to characterise fluctuating fields arising from multifunctional digital electronics in the absence of phase references [6], [7].

In this paper, we consider emissions from a slotted enclosure containing a Galileo[®] micro controller board, a complex digital electronics source that span a broad frequency range from the very high frequency (VHF) to the microwave regime. In

particular, we focus on the low end of the emission spectrum, where significant very high frequency (VHF) components are radiated with wavelengths on the order of meters. We are interested in characterising the radiated emissions in the reactive near-field, and therefore perform NFS a few cm beyond the source plane. Performing NFS a few centimetres away from the source means that deep evanescent waves, *i.e.* a reactive near field, dominate.

Near-to-Far Field (NFF) propagation methods have been used to characterise antennas [8] and circuitry [9], and have recently been extended to broadband complex statistical sources, including mobile phones [10], [11], PCBs [12], [6] and open reverberation chambers [7]. The focus in this work is, however, on studying *Near-to-Near field* (NNF) to understand the role evanescent waves in the propagation of complex, partially coherent, stochastic fields. One approach to wide-bandwidth complex fields is to treat them statistically by measuring the spatial correlation function (CF) of the Device Under Test (DUT), see [13].

In what follows, a NNF transformation of the CF is derived and compared against the measured CF at increasing distances (but small fractions of the wavelength) from a test source. A phase-space representation of the radiation mechanism is obtained through a Wigner Function (WF) transformation of the CF calculated from direct NFS measured fields: this gives a representation of waves in the combined space of their position and direction of propagation, or phase-space [14]. Although Wigner-functions techniques are usually associated with short-wavelength asymptotics and ray tracing, we use them here to interpret the propagated fields in the deep evanescent limit.

It is found that phase space is dominated by large values of a momentum variable. This momentum variable is associated with ray direction in the short-wavelength limit but in the reactive near field dominating the measurements we report, it instead dictates the rate of evanescent decay away from the source. This extends previous work [15, Sec 3.] in which a phase-space propagator has been used to transport weakly evanescent components. The theory is described in Sec. II and is validated in Sec. III using measurements of complex digital electronics radiating inside a metallic enclosure with a narrow aperture. The WF propagation method proves to be a valuable tool to understand local emission directionality at arbitrary frequencies. Propagating densities of evanescent waves in the short range is of interest in source reconstruction, emission source microscopy (ESM) [16] and holography.

G. Gradoni is with the School of Mathematical Sciences and the George Green Institute for Electromagnetics Research, University of Nottingham, University Park, UK.

D. M. Ramapriya, S. C. Creagh, and G. Tanner are with the School of Mathematical Sciences, University of Nottingham, University Park, UK, e-mail: gabriele.gradoni@nottingham.ac.uk.

M. H. Baharuddin is with the George Green Institute for Electromagnetics Research, University of Nottingham, University Park, UK and Department of Electrical Electronic and Systems Engineering, Universiti Kebangsaan Malaysia, 43600 UKM Bangi, Selangor, Malaysia

H. Nasser, C. Smartt, and D. W. P. Thomas are with the George Green Institute for Electromagnetics Research, University of Nottingham, University Park, UK.

II. MODELLING STOCHASTIC FIELDS

Electromagnetic radiation from complex electronics such as highly integrated and multifunctional PCBs varies essentially randomly in both space and time. A statistical approach is then appropriate. As discussed in [7], radiation from such complex sources may be exemplified by aperture scanning of the transverse magnetic fields over planes parallel to the source and calculation of a spectral field-field correlation function.

Let $\psi(\mathbf{x}, z; t)$ denote an in-plane component of the vector EM field radiated from a planar source into the half space $z > 0$, where \mathbf{x} denotes coordinates perpendicular to z . This field is stochastic and its spatial correlation can be defined as

$$C_z(\mathbf{x}_1, \mathbf{x}_2; \tau) = \lim_{T \rightarrow \infty} \frac{1}{T} \int_0^T \psi(\mathbf{x}_1, z; t + \tau) \psi(\mathbf{x}_2, z; t) dt. \quad (1)$$

In the frequency domain, this field-field correlation is represented by the Fourier transform

$$\Gamma_z(\mathbf{x}_1, \mathbf{x}_2; \omega) = \int_{-\infty}^{\infty} e^{-i\omega\tau} C_z(\mathbf{x}_1, \mathbf{x}_2; \tau) d\tau. \quad (2)$$

Furthermore, we note that the correlation function on the source plane $z = 0$ can be represented using an in-plane direction cosine \mathbf{p} as

$$\tilde{\Gamma}_z(\mathbf{p}_1, \mathbf{p}_2) = \iint e^{-ik\mathbf{p}_1 \cdot \mathbf{x}_1} \Gamma_z(\mathbf{x}_1, \mathbf{x}_2; \omega) e^{ik\mathbf{p}_2 \cdot \mathbf{x}_2} d\mathbf{x}_1 d\mathbf{x}_2, \quad (3)$$

where k denotes the free-space wavenumber. Then

$$\tilde{\Gamma}_z(\mathbf{p}_1, \mathbf{p}_2) = e^{ikz[T(\mathbf{p}_1) - T^*(\mathbf{p}_2)]} \tilde{\Gamma}_{z=0}(\mathbf{p}_1, \mathbf{p}_2), \quad (4)$$

where a normal direction cosine is defined ([17], page 342)

$$T(\mathbf{p}) = \begin{cases} \sqrt{1 - p^2} & \text{for } p^2 \leq 1 \\ i\sqrt{p^2 - 1} & \text{for } p^2 > 1, \end{cases} \quad (5)$$

where $p = |\mathbf{p}|$. This applies both to evanescent ($p^2 > 1$) and propagating ($p^2 \leq 1$) regimes. Joint positional and directional information can be extracted from the CF through the WF obtained from (4) by making the coordinate rotation

$$\begin{aligned} \mathbf{p} &= (\mathbf{p}_1 + \mathbf{p}_2)/2, \\ \mathbf{q} &= \mathbf{p}_1 - \mathbf{p}_2 \end{aligned} \quad (6)$$

and then taking an inverse Fourier transform in the displacement variable \mathbf{q}

$$W_z(\mathbf{x}, \mathbf{p}) = \left(\frac{k}{2\pi}\right)^d \int e^{ik\mathbf{x} \cdot \mathbf{q}} \tilde{\Gamma}_z(\mathbf{p}, \mathbf{q}) d\mathbf{q}, \quad (7)$$

where $\mathbf{x} = (\mathbf{x}_1 + \mathbf{x}_2)/2$, and d is the dimension of the transverse scan. In a full 3D simulation, $\mathbf{x} = (x, y)$ and $d = 2$, but we also discuss a simplified analysis in which \mathbf{x} is represented by a single component x and $d = 1$. Both the CF and WF of propagating [7] and weakly evanescent [15] wave densities have been studied extensively for a planar source. An extension of those studies is necessary when scanning in the deep near field at distances very close to complex sources. In this case, the NFS probes are most likely to operate in the *reactive* near field of the source, where evanescent waves dominate. This corresponds to the regime $p^2 \gg 1$ in Fourier

and Wigner representations of the data. Transporting densities of evanescent waves in the short range requires a substantial extension of the leading order propagators derived in [15, Sec. 3.], so as to capture the suppression (and, as we will see, the diffusion) of evanescent waves localised in transverse position \mathbf{x} . An explicit propagator for the WF can be obtained by taking the Wigner transform of the propagated CF, and inverse Fourier transforming the source CF to obtain its associated WF. Propagation is achieved by using (4) in (7). Decay and diffusion of the propagated CF can be captured by noting that the obtained resulting WF propagator [15, Eq. (8)] can be written formally as

$$W_z(\mathbf{x}, \mathbf{p}) = W_{z_0}(\mathbf{x}, \mathbf{p}) *_x \mathcal{G}(\mathbf{x}, \mathbf{p}), \quad (8)$$

where $*_x$ indicates a convolution with respect to the variable \mathbf{x} only, and

$$\mathcal{G}(\mathbf{x}, \mathbf{p}) = \left(\frac{k}{2\pi}\right)^d \int e^{-kz(T(\mathbf{p}+\mathbf{q}/2) - T^*(\mathbf{p}-\mathbf{q}/2))} e^{ik\mathbf{q} \cdot \mathbf{x}} d\mathbf{q}. \quad (9)$$

When the near field is dominated by rapid evanescent decay, we use $|\mathbf{p} + \mathbf{q}/2| \gg 1$ and $|\mathbf{p} - \mathbf{q}/2| \gg 1$ to approximate

$$W_z(\mathbf{x}, \mathbf{p}) \approx W_{z_0}(\mathbf{x}, \mathbf{p}) *_x \mathcal{G}_{\text{evan}}(\mathbf{x}, \mathbf{p}), \quad (10)$$

where

$$\mathcal{G}_{\text{evan}}(\mathbf{x}, \mathbf{p}) = \left(\frac{k}{2\pi}\right)^d \int e^{-kz(|\mathbf{p}+\mathbf{q}/2| + |\mathbf{p}-\mathbf{q}/2|)} e^{ik\mathbf{q} \cdot \mathbf{x}} d\mathbf{q} \quad (11)$$

approximates $\mathcal{G}(\mathbf{x}, \mathbf{p})$. The effect of the convolution with $\mathcal{G}_{\text{evan}}(\mathbf{x}, p)$ is two-fold: there is a \mathbf{p} -dependent decay by a factor e^{-2kpz} in this integrand, and there is a diffusion in \mathbf{x} arising from the convolution operation.

These effects are now described in more detail for the case $d = 1$. This lower-dimensional model captures the dominant effects in the measurements described in the next section showing nearfield decay from a one-dimensional slit. Then the integral (11) can be evaluated explicitly to give

$$\mathcal{G}_{\text{evan}}(x, p) = \frac{e^{-2kpz}}{\pi} \left(\frac{z \cos(2kpx) - x \sin(2kpx)}{z^2 + x^2} + \frac{\sin(2kpx)}{x} \right). \quad (12)$$

A comparison is made for a representative value of p in Fig. 1 between this approximation of the diffusion kernel and a numerical evaluation of (9) in which the full form (5) is used for the normal direction cosine for the one dimensional case. The approximation (12) captures well the overall form of the diffusion kernel and we note that the approximation improves as p increases.

Returning to the general case, the propagated correlation function can be retrieved by performing an inverse Fourier transform of the WF with respect to \mathbf{p} , which is defined as

$$\Gamma_z(\mathbf{x}_2, \mathbf{x}_1) = \left(\frac{k}{2\pi}\right)^d \int e^{ik\mathbf{p} \cdot \mathbf{s}} W_z(\mathbf{x}, \mathbf{p}) d\mathbf{p}, \quad (13)$$

where the position displacement $\mathbf{s} = \mathbf{x}_1 - \mathbf{x}_2$ is the variable conjugate to \mathbf{p} . The intensity I_z as a function of distance from

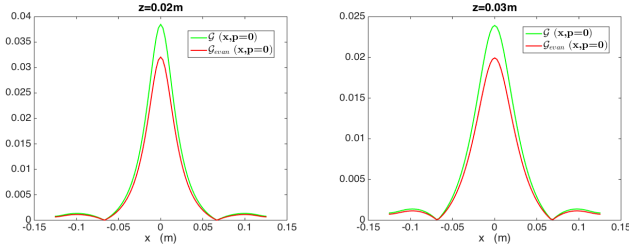


Fig. 1: Comparison between the approximate diffusion kernel $\mathcal{G}_{\text{evan}}(x, p)$ in (12) and the full integral in (9) at selected distances beyond the planar source, $z = 0.02$ m and $z = 0.03$ m, and for $p = 0$

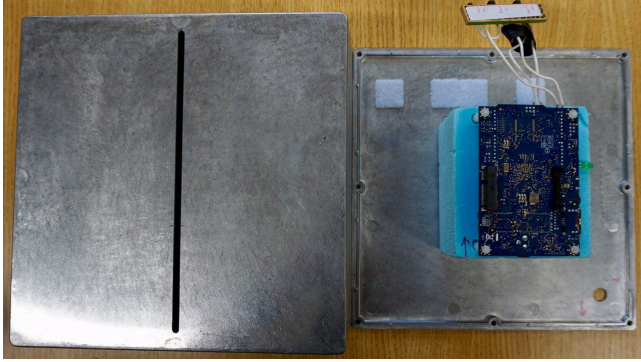


Fig. 2: Slotted enclosure (left) and Galileo micro controller PCB (right) making the DUT: the PCB is positioned inside the enclosure in close proximity to the (inner side of) the slot.

the source is given by

$$I_z(\mathbf{x}) = \Gamma_z(\mathbf{x}, \mathbf{x}) = \left(\frac{k}{2\pi}\right)^d \int W_z(\mathbf{x}, \mathbf{p}) d\mathbf{p}. \quad (14)$$

III. EXPERIMENTAL RESULTS AND VALIDATION

The DUT considered for a verification of the theory is a slotted enclosure equipped with a PCB. The enclosure is an aluminium box of dimensions 0.25 m x 0.25 m x 0.1 m with a laser-cut slit of dimensions 0.22 m by 0.005 m. The PCB is a Galileo[®] micro controller board. Fig. 2 shows geometry and dimensions of both the PCB and the enclosure. An automated dual probe scanning system has been developed and is controlled by a PC while the probes are connected to a 4 channel 8GHz KEYSIGHT DSOS804a Digital Oscilloscope. The source of the EM radiation is a Galileo microcontroller board which is inside the box. The two probes are scanned over a path along the slit where the scan line is 250 mm and with 5 mm steps. The fields obtained through linear NFS of a single in-plane magnetic component at different heights z are then used to calculate the CF using (1) and (2). The two-probe procedure described in [7] was adopted to calculate the CF from space-time fields obtained through linear NFS of a single in-plane magnetic component at different heights z using (1) and (2). The discretisation of (1) and (2), along with an algorithm to compute the discrete WF, is explained in detail in [7]. Measured fields and calculated CF data are obtained at heights of $z = 0.005$ m and $z = 0.02$ m from the source plane.

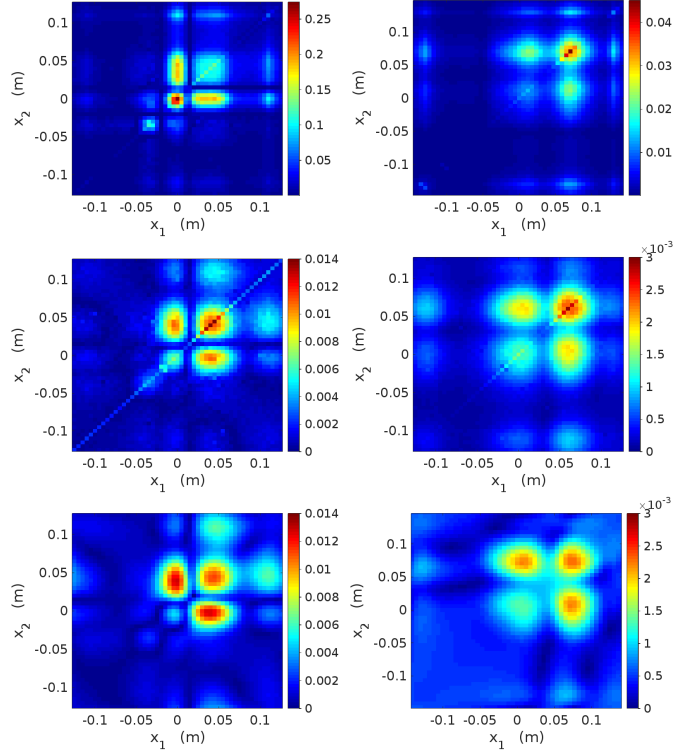


Fig. 3: Measured CFs are shown at the top for 100 MHz (left) and 250 MHz (right) at the height $z = 0.005$ m. The middle row shows corresponding measurements for $z = 0.02$ m. The bottom row shows the corresponding CFs obtained by using the approximate WF propagator in (12) to propagate measured data from $z = 0.005$ to $z = 0.02$ m.

The measured fields are captured as a function of time over a period of 1 ms. It is assumed that the processes of significance happening on the board are included in this time period. In the post processing of the data this time period was divided into an ensemble of 128 shorter time periods. The Fourier Transform of each of these datasets was calculated for the frequencies of interest. The correlation matrix elements were then calculated using (2) from the ensemble of frequency domain data.

The capability of the Galileo to be programmed is a useful feature as we are then able to control the characteristics of the measured fields. In order to emulate a realistic complex source, a memory intensive program has been designed to run on the Galileo: this consists of allocating a large array and then assigning random numbers to random addresses throughout the whole scanning process. The running of this process is found to create significant VHF components. Prior to performing the two-probe NFS, emission of the Galileo board has been observed by probing the magnetic field on components on the Galileo. This results in a broadband response at 100 MHz and 250 MHz which makes it interesting to investigate the field-field correlation at these frequencies. We focus on emission frequencies of 100 MHz and 250 MHz. An experimental WF is obtained through the CF at different heights by applying (7) with $d = 1$.

The source CFs at $z = 0.005$ m are shown in the top

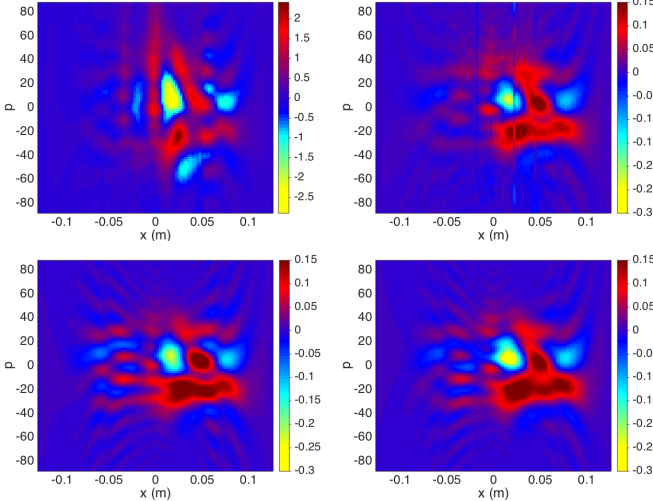


Fig. 4: The WFs obtained from measured data at 100 MHz are shown at top left for $z = 0.005$ m at top right for $z = 0.02$ m. On the bottom left and right are shown the WFs obtained respectively by using the full propagator (9) and its approximation (12) to propagate measured data from $z = 0.005$ to $z = 0.02$ m.

row of Fig. 3 for 100 MHz and 250 MHz. Corresponding measurements for $z = 0.02$ m are shown in the middle row of Fig. 3. The bottom row of that figure shows the CFs obtained by: (i) converting the CF measured at $z = 0.005$ m to a WF; (ii) using the approximation (12) to propagate this WF to $z = 0.02$ m and (iii) using the inverse transform to convert the propagated WF to a CF. Despite the rather simplified approximation used in this process, the propagated CFs agree well with the measured CF's. A diffusive spreading of the hotspots can be observed for both frequencies when moving away from the source.

Greater insight into the propagation mechanism can be obtained by examining the corresponding WFs, which are shown in Fig. 4 for the 100 MHz case. Most of the energy content in the measurements treated here indeed falls outside the strip $-1 < p < 1$ corresponding to components propagating to the farfield, confirming that evanescent components with $|p| > 1$ dominate the nearfield. The evanescent components are significantly suppressed on passing from $z = 0.005$ m to $z = 0.02$ m, even if the shift along the transport coordinate is a small fraction of λ . A more detailed analysis of the wave dynamics is also possible: for example, a striking feature of the propagated CFs in Fig. 3 is that the most intense hotspot of the source data at $z = 0.005$ m, seen near $x = 0$ in the top row of Fig. 3, propagates to a comparatively less intense hotspot at $z = 0.02$ m. In turn, the originally less intense peak near $x = 0.005$ m dominates at $z = 0.02$ m. An explanation for this counterintuitive behaviour can be found in the source WF shown at the top left of Fig. 4. Here the initially higher peak near $x = 0$ is seen to be associated with a vertical stripe in the WF which extends to rather large values of p . Therefore, although the peak near $x = 0$ is initially more intense, it is more deeply evanescent, and so decays faster.

The intensity, Eq. (14), is shown in Fig. 5 for 100 MHz and 250 MHz: the agreement between measured and predicted intensity is satisfactory. From the intensity evolution, we

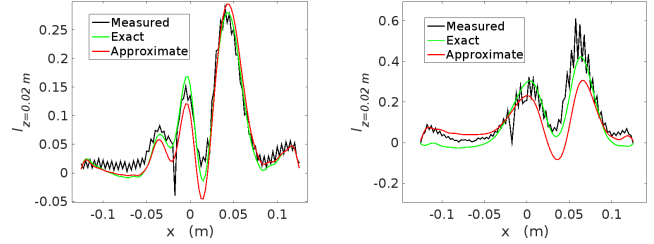


Fig. 5: The intensity at $z = 0.02$ m: measured vs propagated for the frequencies 100 MHz (left) and 250 MHz (right).

see that there is a significant reduction in amplitude as we increase the measurement height from 0.005 m to 0.02 m. The near field approximation described in Eqs. (10)-(12) are less effective when propagated components contribute to radiated emissions, which happens at higher frequencies. This is the cause for the larger discrepancy in Fig. 5 (right). The z range in which evanescent waves dominate is discussed for a simplified model in [15, Fig. 4], and it is defined by a linear increase of the correlation length of the propagated field within $kz < 1$.

IV. CONCLUSION

The Wigner function represents stochastic fields in the position-direction space, or phase-space, and includes the presence of evanescent waves for imaginary emission angles. It can be calculated from the spectral field-field correlation function and its definition is not restricted to the far-field. We observe that very near-field radiated emissions from complex planar sources are transported diffusively within a short range (a fraction of the wavelength) of the source. Synthetic aperture measurements have been performed at different distances from a slotted enclosure equipped with a PCB. A closed-form (approximate) convolution propagator has been derived for the Wigner function, which successfully predicts the observed diffusion of evanescent waves. Such results will assist source reconstruction of arbitrary devices, and improve holographic source reconstruction methods, e.g., emission source microscopy.

ACKNOWLEDGMENTS

Financial support by the COST (European Cooperation in Science and Technology) Action IC1407 ‘‘ACCREDIT’’, and the Horizon 2020 FET network NEMF21 (Grant-Num.: 664828) are gratefully acknowledged. We acknowledge stimulating discussions with Peter Russer (TUM) and Johannes Russer (TUM).

REFERENCES

- [1] X. Tong, D. Thomas, A. Nothofer, P. Sewell, and C. Christopoulos, ‘‘Modeling electromagnetic emissions from printed circuit boards in closed environments using equivalent dipoles,’’ *Electromagnetic Compatibility, IEEE Transactions on*, vol. 52, no. 2, pp. 462–470, May 2010.

- [2] H. Weng, D. G. Beetner, and R. E. DuBroff, "Prediction of radiated emissions using near-field measurements," *IEEE Transactions on Electromagnetic Compatibility*, vol. 53, no. 4, pp. 891–899, Nov 2011.
- [3] Z. Yu, J. A. Mix, S. Sajuyigbe, K. P. Slattery, and J. Fan, "An improved dipole-moment model based on near-field scanning for characterizing near-field coupling and far-field radiation from an ic," *IEEE Transactions on Electromagnetic Compatibility*, vol. 55, no. 1, pp. 97–108, Feb 2013.
- [4] X. Gao, J. Fan, Y. Zhang, H. Kajbaf, and D. Pommerenke, "Far-field prediction using only magnetic near-field scanning for emi test," *Electromagnetic Compatibility, IEEE Transactions on*, vol. 56, no. 6, pp. 1335–1343, Dec 2014.
- [5] J. Fan, "Near-field scanning for em emission characterization," *IEEE Electromagnetic Compatibility Magazine*, vol. 4, no. 3, pp. 67–73, rd 2015.
- [6] J. A. Russer and P. Russer, "Modeling of noisy em field propagation using correlation information," *IEEE Transactions on Microwave Theory and Techniques*, vol. 63, no. 1, pp. 76–89, Jan 2015.
- [7] G. Gradoni, L. R. Arnaut, S. C. Creagh, G. Tanner, M. H. Baharuddin, C. Smartt, and D. W. P. Thomas, "Wigner-function-based propagation of stochastic field emissions from planar electromagnetic sources," *IEEE Transactions on Electromagnetic Compatibility*, vol. PP, no. 99, pp. 1–9, 2017.
- [8] T. K. Sarkar and A. Taaghoul, "Near-field to near/far-field transformation for arbitrary near-field geometry utilizing an equivalent electric current and mom," *Antennas and Propagation, IEEE Transactions on*, vol. 47, no. 3, pp. 566–573, Mar 1999.
- [9] G. Cerri, R. D. Leo, and V. M. Primiani, "A rigorous model for radiated emission prediction in pcb circuits," *IEEE Transactions on Electromagnetic Compatibility*, vol. 35, no. 1, pp. 102–109, Feb 1993.
- [10] B. Fourestie, Z. Altman, J.-C. Bolomey, J. Wiert, and F. Brouaye, "Statistical modal analysis applied to near-field measurements of random emissions," *Antennas and Propagation, IEEE Transactions on*, vol. 50, no. 12, pp. 1803–1812, Dec 2002.
- [11] B. Fourestie, J.-C. Bolomey, T. Sarrebourg, Z. Altman, and J. Wiert, "Spherical near field facility for characterizing random emissions," *Antennas and Propagation, IEEE Transactions on*, vol. 53, no. 8, pp. 2582–2589, Aug 2005.
- [12] L. R. Arnaut and C. S. Obiekezie, "Comparison of complex principal and independent components for quasi-gaussian radiated emissions from printed circuit boards," *IEEE Transactions on Electromagnetic Compatibility*, vol. 56, no. 6, pp. 1598–1603, Dec 2014.
- [13] C. Smartt, D. W. P. Thomas, H. Nasser, M. Baharuddin, G. Gradoni, S. C. Creagh, and G. Tanner, "Challenges of time domain measurement of field-field correlation for complex pcbs," in *2015 IEEE International Symposium on Electromagnetic Compatibility (EMC)*, Aug 2015, pp. 953–958.
- [14] N. Marcuvitz, "The quasiparticle view of wave propagation," *Proceedings of the IEEE*, vol. 79, no. 10, pp. 1350–1358, Oct 1991.
- [15] G. Gradoni, S. C. Creagh, G. Tanner, C. Smartt, and D. W. P. Thomas, "A phase-space approach for propagating field-field correlation functions," *New Journal of Physics*, vol. 17, no. 9, p. 093027, 2015.
- [16] P. Maheshwari, H. Kajbaf, V. V. Khilkevich, and D. Pommerenke, "Emission source microscopy technique for emi source localization," *IEEE Transactions on Electromagnetic Compatibility*, vol. 58, no. 3, pp. 729–737, June 2016.
- [17] G. Barton, *Elements of Green's Functions and Propagation: Potentials, Diffusion, and Waves*, ser. Oxford science publications. Clarendon Press, 1989.